NASA/CR-2001-211020
ICASE Report No. 2001-18

Free-form Airfoil Shape Optimization Under Uncertainty Using Maximum Expected Value and Second-order Second-moment Strategies

Luc Huyse
ICASE, Hampton, Virginia

ICASE
NASA Langley Research Center
Hampton, Virginia

Operated by Universities Space Research Association

National Aeronautics and
Space Administration

Langley Research Center
Hampton, Virginia 23681-2199

Prepared for Langley Research Center
under Contract NAS1-97046

June 2001

FREE-FORM AIRFOIL SHAPE OPTIMIZATION UNDER UNCERTAINTY USING MAXIMUM EXPECTED VALUE AND SECOND-ORDER SECOND-MOMENT STRATEGIES

LUC HUYSE*

Abstract. Free-form shape optimization of airfoils poses unexpected difficulties. Practical experience has indicated that a deterministic optimization for discrete operating conditions can result in dramatically inferior performance when the actual operating conditions are different from the - somewhat arbitrary - design values used for the optimization. Extensions to multi-point optimization have proven unable to adequately remedy this problem of "localized optimization" near the sampled operating conditions. This paper presents an intrinsically statistical approach and demonstrates how the shortcomings of multi-point optimization with respect to "localized optimization" can be overcome. The practical examples also reveal how the relative likelihood of each of the operating conditions is automatically taken into consideration during the optimization process. This is a key advantage over the use of multipoint methods.

Key words. airfoil shape optimization, sensitivity analysis, statistical decision making, robust design, stochastic optimization, second moment analysis, expected value optimization, multi-point optimization

Subject classification. Applied and Numerical Mathematics

1. Introduction. The design process of a structure or device is essentially a decision-making process. Appropriate values of design variables, which optimize the performance of the design, need to be selected. The specification of one or more design operating conditions allows the engineer to use deterministic optimization schemes. An example hereof is found in airfoil design where a cruise Mach number and target lift coefficient are specified and the objective is to minimize the drag under those constraints.

Optimization of an analytical model is a tool to develop better designs. Recent advances in computing power and the development of more accurate computational fluid dynamics codes (CFD) should, at least in theory, allow one to compute the optimal shape of an airfoil for a particular application. Unfortunately, the use of deterministic optimization techniques leads to unexpected problems and often unacceptable results.

An important concern in the shape optimization of airfoils is the sensitivity of the final optimal design to small manufacturing errors or fluctuations in the operating conditions. Tightening the tolerances in the manufacturing process may prove prohibitively expensive or practically impossible to achieve. It is expensive to produce such a precision design and impossible to maintain this pristine shape during routine flight operations. Moreover, a certain variability in the operating conditions (e.g. cruise Mach number) cannot be avoided. The sensitivity of the design performance to relatively small uncertainties provides an incentive to use so-called "robust" optimization methods, which directly assess the effects of the uncertainties on the design performance.

Several different non-deterministic approaches (Taguchi methods, bounds-based, minimax, fuzzy and probabilistic methods) can be taken to achieve "robustness". This research deals with robust design of airfoils. Other researchers have worked in the field of reliability-based design, and have demonstrated optimization of aerospace structures (e.g. [7]). Figure 1.1 explains the difference between robust and reliability-based design

*ICASE, Mail Stop 132C, NASA Langley Research Center, Hampton, VA 23681-2199 (email: l.huyse@larc.nasa.gov). This research was supported by the National Aeronautics and Space Administration under NASA Contract No. NAS1-97046 while the author was in residence at ICASE, NASA Langley Research Center, Hampton, VA 23681-2199.

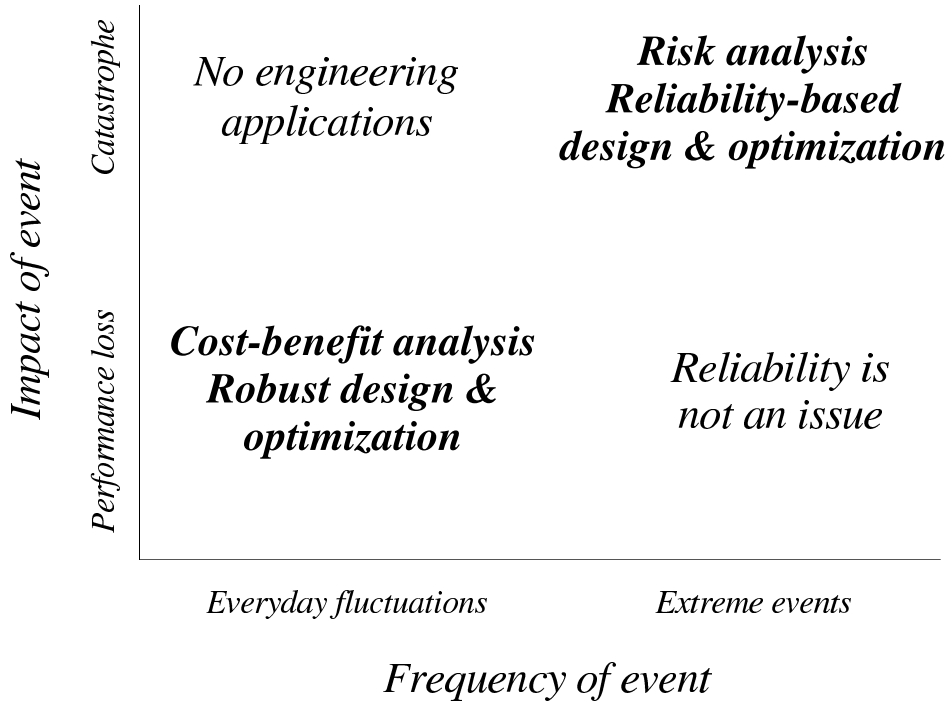

FIG. 1.1. *Uncertainty classification*

problems. In an engineering context, risk is typically defined as the product of the probability and the impact or consequence of an event [16]. Structural reliability techniques are particularly useful to assess the risk associated with infrequent but potentially catastrophic events (such as turbine blade failures [1]). On the other hand, robust optimization techniques account for the impact of everyday fluctuations of parameters (such as variations in operating speed) on the overall design performance assuming that no catastrophic failures occur.

2. Achieving "Robustness". Developing optimization methods which result in more "robust" designs sounds appealing. The term "robustness" has been coined to mean a variety of things. This section outlines some of the more popular goals of "robust" design. Loosely speaking we can distinguish the following meanings:

1. Identify designs which minimize the variability of the performance under uncertain operating conditions. This is the objective of Taguchi methods [12]; they are most practical when the mean value of the performance can be adjusted at negligible cost.
2. Mitigate the detrimental effects of the worst-case performance. This is the objective of MiniMax strategies [23]. They choose the design with the "best" worst-case performance.
3. Provide the best overall performance over the entire lifetime of the structure or device [20]. This is the objective of this work.

In the remainder of this paper the focus is on the third definition: robust optimization which tries to achieve the best performance (or minimal cost) for all possible combinations of the operating conditions. The paper focuses on the effectiveness of the optimization strategy rather than on particular implementations of optimization algorithms.

To our knowledge, non-deterministic approaches are quite new to aerodynamic optimization. First, an overview of existing deterministic attempts at introducing robustness is presented. Subsequently, we introduce an inherently statistical approach based on Van Morgenstern's Maximum Expected Value Criterion [20]. Numerical results for a 2D airfoil shape optimization problem obtained using the different optimization strategies are compared.

3. Airfoil Optimization Problem in Transonic Regime.

3.1. Problem Formulation. In this section we present a transonic airfoil optimization problem to which the various optimization strategies will be applied. All optimizations use the NACA-0012 profile as the baseline geometry. The NACA-0012 is splined using 23 control nodes. The design variables in the optimization problem are given by the vertical positions of the control nodes and the angle of attack α. Three control nodes are in locked positions: one at the leading edge, and a double control node at the trailing edge. Box constraints limit the maximum movement of each of the 20 spline control nodes (see Figure 3.1). The inviscid Euler equations for the flow are discretized on unstructured meshes [4]. The sensitivities of both lift and drag with respect to the design parameters are efficiently calculated using a discrete adjoint formulation [3].

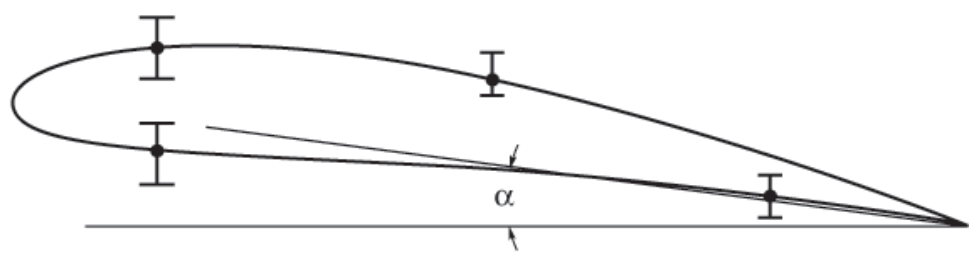

FIG. 3.1. *Design variables and box constraints for the airfoil*

The objective is lift-constrained ($C_l \geq C_l^*$) minimization of the drag C_d over the Mach range $M \in [0.7, 0.8]$.

$$\begin{cases} \min_{\mathbf{d}\in\mathbf{D}} \; C_d(\mathbf{d}, M) \text{ over } M \in [0.7, 0.8] \\ \text{subject to } C_l \geq C_l^* \end{cases} \tag{3.1}$$

where $\mathbf{d}$ is the vector of design variables and $\mathbf{D}$ is the design space. In this study, the Mach number is the only uncertain operating variable; no additional model uncertainties are included. No constraints are imposed on the pitching moment C_m. Because the NACA-0012 is not suitable for the transonic regime, substantial improvements are to be expected, especially when the target lift C_l^* is relatively high.

3.2. Grid Convergence. Four different grid resolutions were used to check the convergence of the flow solution, especially the drag C_d. The far field boundary for grid 1 (Figure 3.2) is located at 10 chord lengths. For grids 2, 3 and 4 (see Figures 3.3, 3.4, and 3.5) the far field boundary is located at 50 chord lengths. For each of the grids the number of elements along both the airfoil inner boundary and the circular far field boundary are specified in Table 1. Grid generator details are given in [18]. Figure 3.6 shows the drag-profile in the Mach-range $M \in [0.7, 0.8]$ for a constant angle of attack $\alpha = 1.5^o$. Grids 1and 2 are considered low-fidelity models, while grid 4 is the high-fidelity or "truth" model. To limit the computational

cost, only grids 1 and 2 will be used for the actual optimizations. Upon completion of the optimization a check using grids 3 or 4 can be performed. The idea is to use the fast low-fidelity grids as much as possible, but to verify the results using the high-fidelity grids [2].

TABLE 3.1
Grids used in examples (Grid 1 is generated using Double9, all other grids are generated using AFLR [18])

	Airfoil elem.	Far field elem.	Nodes	Faces	Elements
Grid 1	129	32	411	1170	822
Grid 2	124	32	3060	9025	6120
Grid 3	250	64	9246	27424	18492
Grid 4	500	128	32067	95574	64134

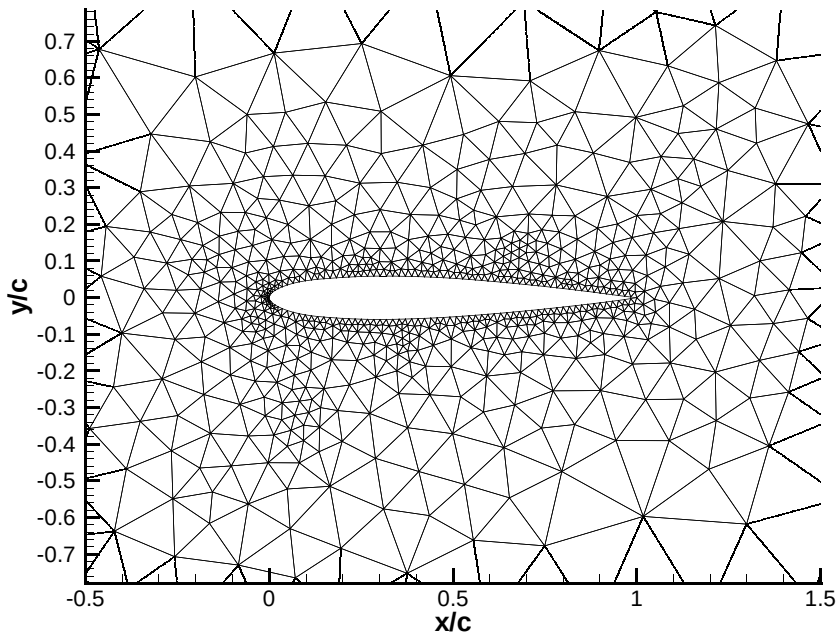

FIG. 3.2. *Baseline NACA-0012 Airfoil: Grid 1*

Figure 3.6 reveals that grids 1 and 2 overestimate the drag. The overestimation of grid 1 has a double cause: it is an extremely coarse grid and the far-field boundary is located at 10 chord lengths only. The overestimation in grid 2 is less than for grid 1 and occurs in equal amounts irrespective of the Mach number. There is virtually no difference in the drag profiles computed on grids 3 and 4. Very similar grid-induced differences in the drag profiles were observed in the Mach sweep curves (C_d as a function of M) for the optimized airfoils.

3.3. Constraint Handling. In this problem we are not concerned with rapid Mach number variations. Only slowly varying Mach numbers (steady states) are considered. Because the Mach number is stable, the angle of attack can be adjusted to reach the required lift C_l^*. Consequently, the constraint in Eq.(3.1) is not probabilistic but remains deterministic. If point-in-time fluctuations are considered, the angle of attack can

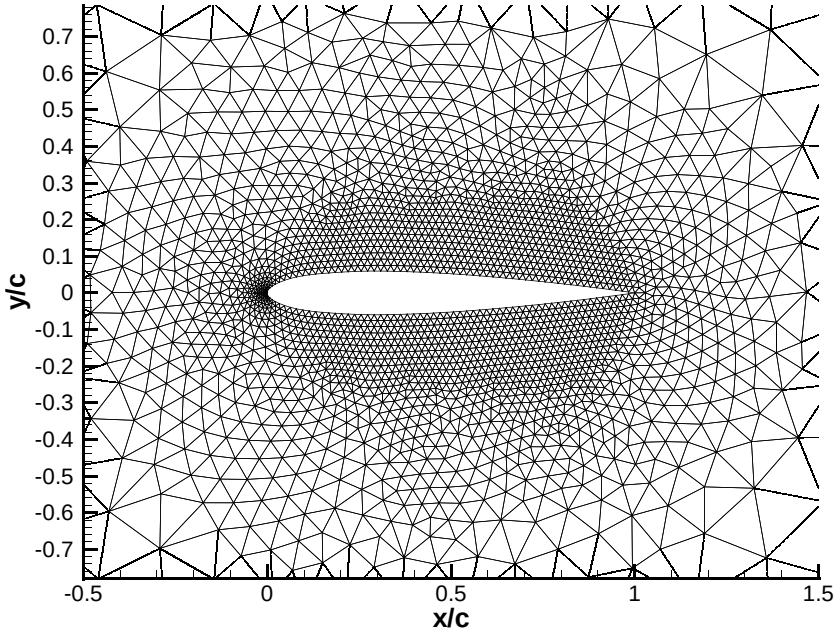

FIG. 3.3. *Baseline NACA-0012 Airfoil: Grid 2*

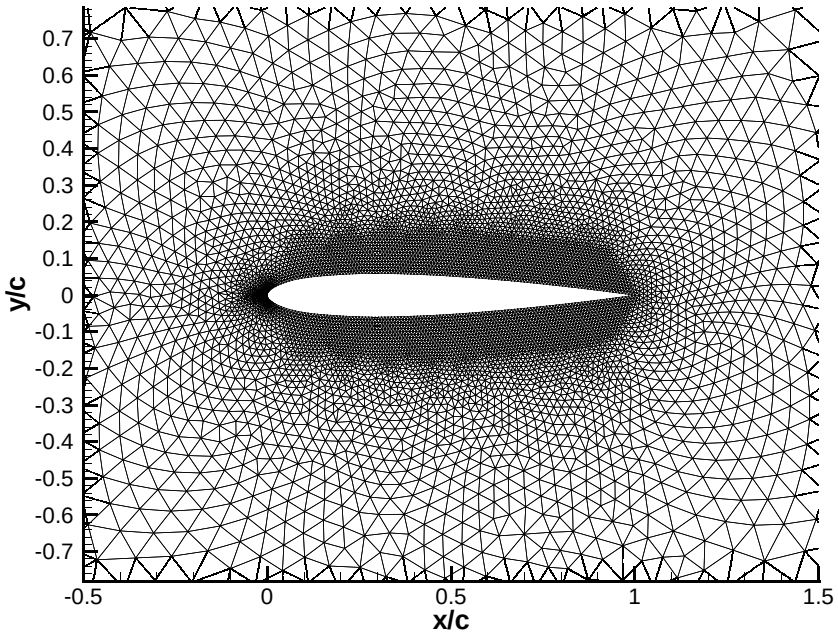

FIG. 3.4. *Baseline NACA-0012 Airfoil: Grid 3*

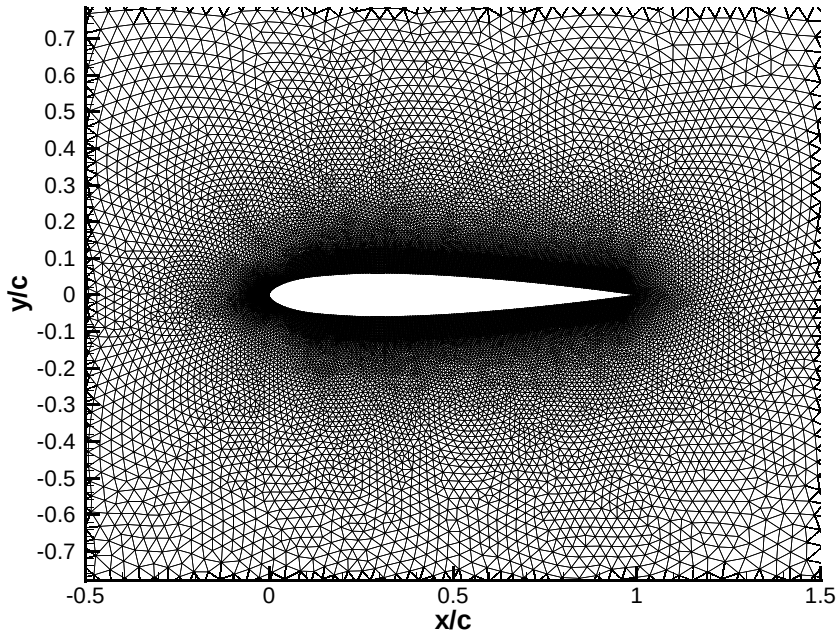

FIG. 3.5. *Baseline NACA-0012 Airfoil: Grid 4*

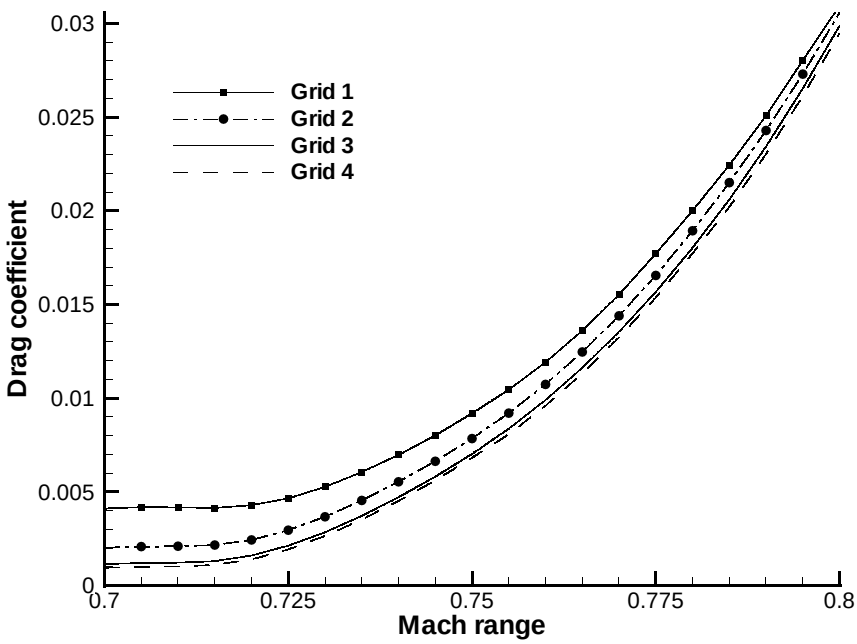

FIG. 3.6. *Drag profiles for NACA-0012 on all 4 grids* ($\alpha = 1.5^o, C_l^* = 0.175$)

no longer be adjusted to assure that enough lift is provided. The constraint needs to be transformed into a probabilistic constraint, which can only be met with a specified probability.

A mathematically straightforward approach to the optimization problem is to account for the inequality constraint in Eq.(3.1) using a feasible direction search algorithm. For this purpose, we linked FUN2D [4] to several optimizers – Modified Method of Feasible Directions (CONMIN) and Sequential Linear Programming (ADS/SLP) – in iSIGHT v.5.5, a product of Engineous Software Inc.[11]. However, the lift constraint can also be eliminated if we take advantage of the specific nature of the problem. We solved the resulting unconstrained optimization problem using PORT, a bound constrained trust region algorithm [14].

4. Deterministic Approach to Airfoil Shape Optimization.

4.1. Formulation of Deterministic Optimization Problem: Single-Point Optimization. In a deterministic context, aerodynamic shape optimization of airfoils is concerned with obtaining the most aerodynamically favorable geometry for fixed – either known or assumed – operating or design conditions. Consider the practical case where the drag C_d is to be minimized at a given, fixed free flow Mach number M:

$$\begin{cases} \min_{\mathbf{d}\in\mathbf{D}} \; C_d(\mathbf{d}, M) \\ \textit{subject to } C_{l,i}(\mathbf{d}, M) \geq C_l^* \quad \textit{for } i = 1, ..., n \end{cases} \tag{4.1}$$

This deterministic, single-point optimization model is not necessarily an accurate reflection of the reality. The formulation in Eq.(4.1) contains no information regarding off-design condition performance. It is documented by other researchers [9] that, with formulation Eq.(4.1), the drag reduction is attained only over a narrow range of Mach numbers (see Figure 4.1a). We will refer to this in the remainder as "localized optimization". Drela explains that the optimizer creates a "bump" on the airfoil to fill the transitional separation bubble (see Figure 4.1b). This effectively reduces the drag penalty which occurs when a bubble undergoes transition and reattachment [8]. However, the location of this bubble varies with M and this explains the poor behavior in off-design conditions for this "locally optimized" design.

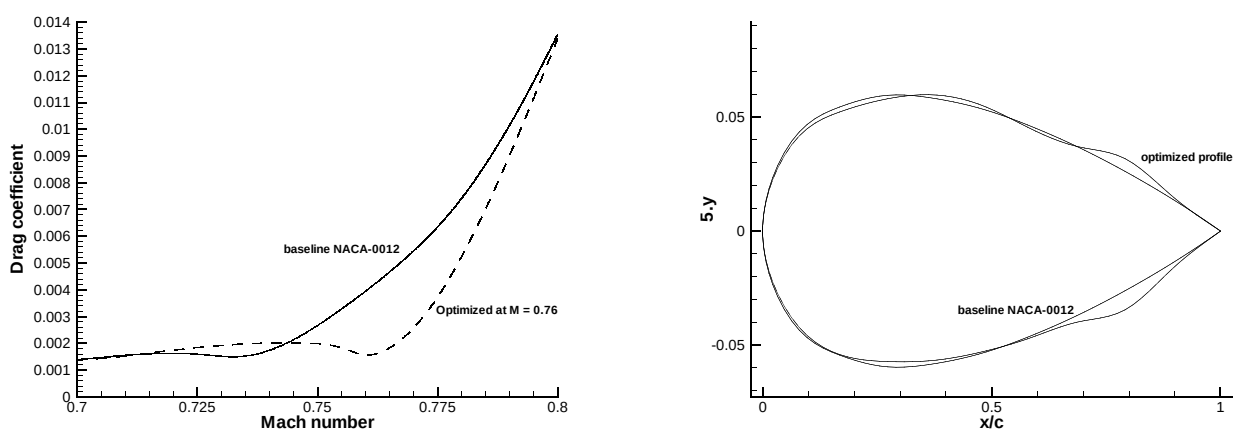

FIG. 4.1. *Single point optimization using Grid 2 and $C_l^* = 0.2$: drag profile and airfoil geometry*

It can be concluded that the real problem is not with the optimization code, which is likely to perform just fine, but with the problem formulation of Eq.(4.1). The "local" optimization effect is particularly

worrisome if substantial variability is associated with the operating conditions. Trade-offs between different design conditions should explicitly be considered in the problem formulation.

4.2. Multi-Point Optimization. A straightforward, but heuristic, approach to avoid point-optimized designs is to consider different Mach numbers and to generalize the objective in Eq.(4.1) to a linear combination of flight conditions (m in total):

$$\begin{cases} \min_{\mathbf{d}\in\mathbf{D}} \sum_i^m w_i C_d(\mathbf{d}, M_i) \\ subject\ to\ C_{l,j}(\mathbf{d}, M_i) \geq C_l^* \quad for\ j = 1, ..., n \end{cases} \tag{4.2}$$

Practical problems arise with the selection of the flight conditions M_i and with the specification of the weights w_i. There is no clear theoretical principles to guide the selection, which is in fact largely left up to the designer's discretion (see e.g. Refs. 6, 9 and 10).

With the multi-point formulation of Eq.(4.2), an improved C_d can be realized over a wider range of Mach numbers M [9]. However, this formulation is still unable to provide a truly global solution by avoiding localized optimization. In fact multiple "bumps" appear on the airfoil, one associated with each flight condition M_i. In the transonic regime, each bump occurs at the shock foot location for each of the sampled Mach numbers.

A clear example of "localized optimization" is given in Figure 4.2. This optimization was performed on Grid 2, with lift constraint $C_l^* = 0.4$, using equal weight ($w_i = 0.25$) for each design condition. Because the drag is highest at the higher Mach numbers, the drag at those Mach numbers has been reduced significantly during the optimization process. Figure 4.2 clearly indicates that these drag improvements occur only at particular Mach numbers and are rapidly lost when the actual Mach number deviates from any of the selected design Mach numbers.

Figure 4.3 explains this in more detail using 2 contour plots of the local Mach number. The operating conditions (free flow Mach numbers) are very similar but the flow solutions (local Mach number) are very different. The multi-point optimization process introduces geometric features to the airfoil which lock the shock waves in place. Since we used four point optimization, we have 4 shocks (see also [9]). In the figure on the left, four shocks can be distinguished along the top surface. In the figure on the right, the most-aft shock has basically disappeared. The optimizer has locally modified the geometry and eliminated the shock associated with Mach 0.8, which was one of the design conditions.

4.3. Heuristic Approach: Weighted Average of Geometries. Since derivatives have to be calculated for each variable at various operating conditions, the computational cost associated with multi-point optimization using CFD is substantial. Knowledge-based methods, which incorporate some "common-sense engineering knowledge" into the optimization process, may be a valuable and cheaper alternative. One such example is the method of the Weighted Average of Geometries (WAG) [6].

In this method the optimal design is obtained as a weighted average of n single-point optimal designs, each one of them corresponding to one of the n chosen operating conditions. The weighting factors depend on the relative importance of each operating condition (similar to the w_i's in Eq.(4.2) in multipoint design) and on the assumptions made regarding the variation of the drag with geometry and Mach number (response surface model).

The method is computationally efficient, but suffers some of the same drawbacks as the multi-point optimization:

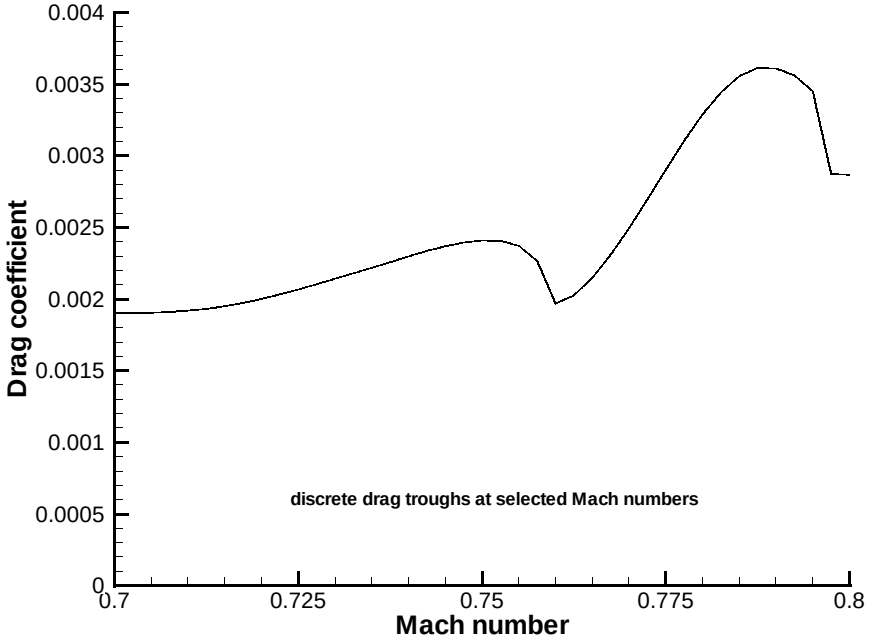

FIG. 4.2. *Drag profile for a four-point optimization using Grid 2 and* $C_l^* = 0.4$*, sample points are* $M = 0.7, 0.733, 0.766$ *and* $M = 0.8$

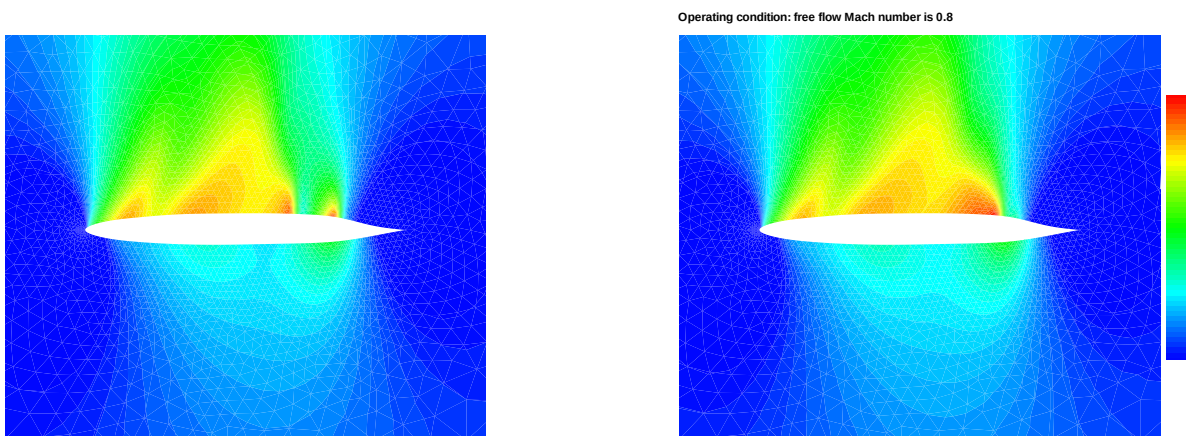

FIG. 4.3. *Local Mach number for two free flow conditions after 4-point optimization using Grid 2 and* $C_l^* = 0.4$

1. As with multi-point optimization, the selection of design conditions to be included in the optimization process is arbitrary.
2. Single point optimizations result in bumpy airfoils. Linear combinations of bumpy airfoils will remain bumpy.
3. Campbell [6] assumes a quadratic variation of C_d with the geometry. This assumption may become

questionable when the geometries are much different due to large variations in Mach number.

5. Non-Deterministic Approaches.

5.1. Design as a Decision-Making Process. Designing a structure or device is essentially a decision-making process. Appropriate values of the design variables $\mathbf{d}$ need to be selected which optimize the performance or the utility of a design. The designer has full control over the design variables, such as the geometry of the structure and the type and grade of materials used for it, but the operating conditions of a structure or device, such as the loads or the operating speeds, will typically vary during the design life time.

Since each operating condition parameter may take on a range of values over the lifetime of the design, it is possible to collect their histograms (and joint histograms). From a subjectivist point of view, the operating conditions θ are then effectively modeled as random variables.

The previous section indicated that a specific design may perform exceptionally well for a selected operating condition, say the free flow Mach number M, but may perform poorly for slightly different values of M, which are quite likely to occur. The impact of the uncertainty of M on the design performance should be taken into account when the quality of a particular design is assessed.

5.2. Bounds-Based Methods. Bounds-based methods recognize that a designer does not have access to data with unlimited precision: some of these data are intrinsically variable (operating conditions), some of them can be collected or measured with limited precision only (sampling error), and sometimes the measurement process itself is imperfect which introduces bias. Gu et al. [13] recognize that analytical and numerical models fail to yield the "correct" result; they call the difference between the average experimental data and the value obtained from the analysis code the bias error. All other errors are lumped into "random variability". They assign bounds to each of those uncertainties and develop a methodology to incorporate the bounds directly into the multi-disciplinary optimization [5].

In our opinion, the main drawback of bounds-based methods is that they essentially assume that all outcomes within the specified bounds are equally likely to occur. This conflicts with the intuitive sense that, by their very definition, extremes should occur with much lower frequency than average or "normal" behavior. This implies that error bounds will grow quite rapidly as more and more uncertainties are explicitly considered in the design or optimization process. An explicitly statistical approach takes the relative likelihood of combined extremes versus other joint occurrences into account by means of the Probability Density Function (PDF). In short two problems can be associated with the bounds-based approach:

1. Bounds cannot always be identified accurately.
2. Bounds-based methods are over-conservative.

5.3. Explicitly Statistical Problem Formulation. Reconsider the basic problem in Eq.(3.1): minimize the drag C_d over a range of free flow Mach numbers M while maintaining lift $C_l \geq C_l^*$. Note that M is now treated as a random variable. The optimization problem Eq.(4.1) is now interpreted as a statistical decision-making problem.

In the presence of uncertainty a designer is forced, in effect, to take a gamble. Under such circumstances, rather than naively hoping for the best or over-conservatively focusing on the worst, the right decision consists in the best possible choice of the design, whether favorable or unfavorable operating conditions occur. All decision problems have two essential characteristics [20]:

1. A choice, or sequence of choices, must be made among various possible designs.
2. Each of these choices corresponds to a performance, but the designer cannot be sure a priori what this performance will be. The exact performance also depends in part on unpredictable events, in

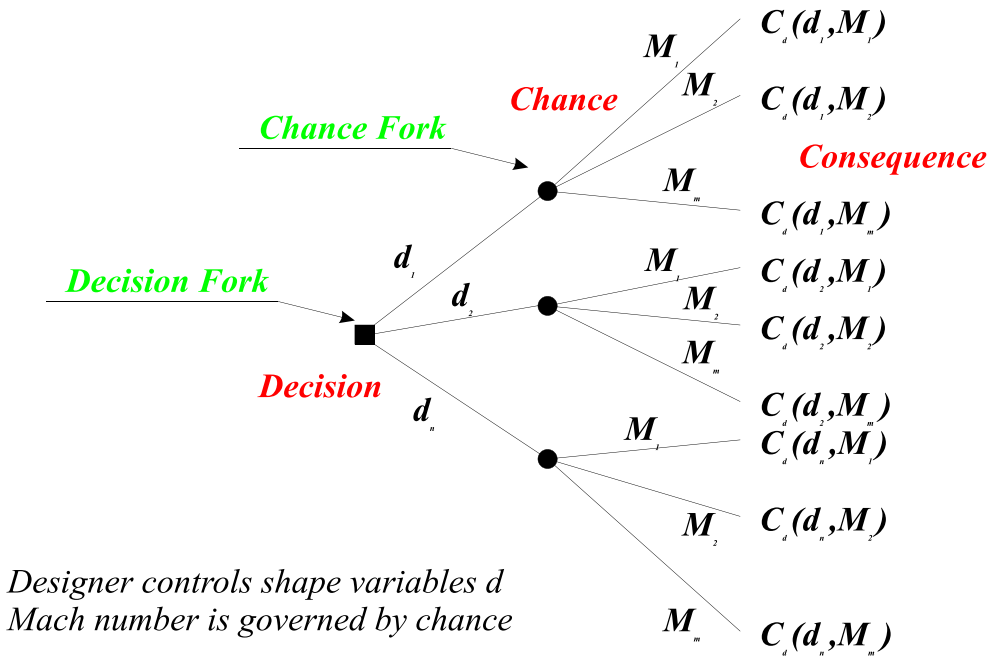

FIG. 5.1. *Decision tree example*

this case the operating conditions.

In our example, only one initial choice (i.e. airfoil selection) regarding the design needs to be made (see Figure 5.1). However, the method is easily extended to accommodate sequential decisions. For instance, we may want to run some wind tunnel experiments in the hope of reducing the uncertainty on some mathematical model predictions. A decision tree would indicate if the upfront cost of the prototypes is offset by the expected reduction in parameter uncertainty.

According to the Von Neumann-Morgenstern statistical decision theory [20], the best course of action in the presence of uncertainty is to select the design which leads to the lowest expected drag. This is commonly known as the Maximum Expected Value criterion (MEV). The risk ρ, associated with a particular design $\mathbf{d}$, is identified as the expected value of the perceived loss associated with the design. The best design or decision, which minimizes the overall risk, is referred to as the "Bayes' decision". In our problem formulation, the Bayes' risk ρ^* and Bayes' decision $\mathbf{d}^*$ are given bu (5.1) and (5.2) respectively:

$$\begin{cases} \rho^* = \min_{\mathbf{d}\in D} \int_M C_d(\mathbf{d}, M) f_M(M) dM \\ \text{subject to } C_l(\mathbf{d}, M) \geq C_l^* \end{cases} \tag{5.1}$$

or

$$\rho^* = \int_M C_d(\mathbf{d}^*, M) f_M(M) dM \tag{5.2}$$

where $f_M(M)$ is the probability density function of the free flow Mach number M.

The practical problem with formulation Eq.(5.1) is that integration is required in each of the optimization steps. Since the objective function C_d is computationally expensive to evaluate, this approach, although theoretically sound, becomes prohibitively expensive. Therefore a computational scheme that minimizes the number of function calls is desirable.

5.4. Analytic Approximation of the Expectation Integral. When the variability of the free flow Mach number M is not too large, a second-order Taylor series expansion of C_d around the mean value $\overline{M}$ may be a sufficiently accurate model of the variation of the drag C_d with respect to M.

$$C_d(\mathbf{d}, M) = C_d(\mathbf{d}, \overline{M}) + \nabla_M C_d.(M - \overline{M}) + \tfrac{1}{2}\nabla_M^2 C_d.(M - \overline{M})^2 \tag{5.3}$$

When substituted in the Bayes' risk expression (5.1), the linear term $\nabla_M C_d.(M - \overline{M})$ in Eq.(5.3) disappears after integration over M because the Taylor series is built around the mean value $\overline{M}$. The Bayes' risk is:

$$\begin{cases} \rho^* = \min_{\mathbf{d}\in D}\left[C_d(\mathbf{d}, \overline{M}) + Var(M)\ \frac{\partial^2 C_d}{2\partial M^2}\Big|_{\mathbf{d},\overline{M}}\right] \\ \text{subject to } C_l(\mathbf{d}, M) \geq C_l^* \end{cases} \tag{5.4}$$

where $Var(M)$ denotes the variance of the Mach number M.

It seems that we have substituted an integration with an almost equally expensive computation of a second-order derivative. Even though the approximation may result in only moderate computational savings, this theoretical result provides additional insight into the problem. It follows from Eq.(5.4) that the variability of M can affect the optimal design only if the objective function C_d is highly non-linear in this parameter. This is the case near the drag divergence Mach number M_{DIV}, where the drag undergoes a sharp increase (recall Figure 4.1a).

In mathematical terms, the advantage of working with expected utilities is that the minimum is second-order accurate with respect to variations in the parameters. This ensures a more global solution and "localized optimization" will be avoided. This can also be explained in an intuitive manner: the second-order derivative is a measure for the curvature. Since this curvature is now a part of the objective function, a design which results in a drag trough or "cusp" as found in the optimal solution in Figure 4.1 will not be accepted by the optimizer. The high curvature of the "cusp" would increase the objective in Eq.(5.4) and excessive localized optimization will be avoided.

5.5. Direct Numerical Evaluation of Expectation and Comparison with Multi-Point Optimization. The integration with respect to M in Eq.(5.1) can also be performed numerically. Irrespective of the chosen integration scheme, the integral (5.1) can formally be written as (n_k integration points):

$$\rho^* = \min_{\mathbf{d}\in D}\left(\sum_{k=1}^{n_k} w_k.C_d(\mathbf{d}, M_k) + \epsilon(n_k)\right) \tag{5.5}$$

where the integration error $\epsilon(n_k) \to 0$ as $n_k \to \infty$.

Formulation Eq.(5.5) is strikingly similar to Eq.(4.2). It is therefore interesting to analyze how the Bayes' decision $\mathbf{d}^*$ compares with the multi-point solution and exactly how localized optimization is avoided.

In the multi-point approach the Mach numbers and weights need to be selected by the designer. In the statistical approach, the weights are directly related to the relative importance of each Mach number through the integration over the probability density. Which Mach numbers are used in the optimization depends on the chosen integration scheme. In short, the statistical approach removes the arbitrariness from the weighting process.

Careful comparison of Eq.(4.2) with Eq.(5.5) reveals the shortcoming in the multi-point formulation which causes localized optimization. Numerical integration of Eq.(5.1) results in Eq.(5.5) and includes a random, zero-mean error term $\epsilon(n_k)$, which decreases as the number of sampling points increases. The multi-point optimization Eq.(4.2) differs from Eq.(5.5) only in the sense that this error term is not explicitly considered in the objective function. However, omitting this error term from the optimization problem alters the structure of the problem at hand. The multi-point optimization effectively looks for the design, which minimizes the weighted sum of the goal function C_d, evaluated in the n_k specified points M_k. There is absolutely no control over what happens to the objective function C_d in the neighborhood around these n_k sampling points. During the optimization iterations, the shape of the goal function $C_d(\mathbf{d}, M)$ is altered. As a result, the discrete sum in Eq.(4.2) may fail to be a good approximation of the integral in Eq.(5.1).

In effect, multi-point optimization will prefer a design $\mathbf{d}_1$ over a design $\mathbf{d}_2$ even when design $\mathbf{d}_1$ is considerably worse than design $\mathbf{d}_2$ in all but the n_k specified sampling points. Multi-point optimization allows the optimizer to mold the goal function C_d to its own advantage. What was originally a random integration error is no longer random, and the discrete sum in Eq.(4.2) no longer approximates the integral in Eq.(5.1) at all.

This rather annoying behavior is avoided if we can prevent the optimizer from exploiting the approximation error in Eq.(5.5) to its own advantage. We need to make sure that the discrete sum in Eq.(5.5) really is an approximation of the integral in Eq.(5.1) at all times. In general terms, we need to ensure that the discrete sum Eq.(4.2) remains a good approximation of the integral in Eq.(5.1). An elegant solution is to randomize the sampling points M_k in the evaluation of the integral but any adaptive optimization scheme that varies the location of the integration points M_k for each optimization step will do. Randomization of the integration points ensures that the optimizer maximizes the performance not just for n_k specific values of M_k, but for any set of values $M_k, k = 1, \ldots n_k$. To minimize the loss of accuracy in the integration due to random location of the integration points, stratified sampling can be used to generate the M_k values. Our experience with the spline-based integration also suggests that the sampling points should not be allowed to be arbitrarily close to each other.

5.6. Additional Considerations. The use of Eq.(5.5) for the optimization instead of Eq.(4.2) leads to numerical complications. Because of the random location of the integration points M_k, a repeated evaluation of the objective function C_d for identical values of the design parameters $\mathbf{d}$ will lead to different results. This makes it hard to identify whether a new design is really better than a previous one, or if the "improvement" should be attributed to random fluctuations instead. When a trial solution $\mathbf{d}$ is still far away from the optimal solution $\mathbf{d}^*$, large improvements ΔC_d can be expected. This means that a very crude integration, which requires very few function evaluations, will suffice in the early stages of the optimization. The improvement of the goal function is expected to be smaller closer to the optimal solution, and more sampling points M_k will be required to keep the integration error small enough. Current research focuses on the development of a strategy which takes maximum advantage of this effect.

In addition, the physical and mathematical models themselves used for the objective function will not be error-free. Each of these model errors can be treated as a random variable. Their effect on the optimal solution is readily assessed by extending the integration over these additional random variables. It is believed that the approximate second-order result in Eq.(5.4) will prove particularly useful for this purpose. In a first step we minimize the drag while keeping the model parameters fixed at their average level. If the second order derivative of the drag with respect to this model parameter at the solution of this simplified problem (without explicit error modeling) is sufficiently small, it can be concluded that these model uncertainties

will only have a minimal impact on the solution. Otherwise, the model uncretainties should explicitly be included in the problem formulation and a full integration is required.

6. Application to a 2D-Airfoil in Transonic Regime.

6.1. Various Optimization Strategies. In this section we compare results for the various optimization strategies presented in this paper. We apply the optimization techniques to the lift-constrained airfoil optimization problem introduced earlier. In this example we assume that the Mach number variations are bounded between 0.7 and 0.8. In particular, the following optimization formulations are compared:

1. Optimization at a single Mach number: various Mach numbers are considered as the design point.
2. Multipoint optimization using m Mach numbers. Each of the design conditions has pre-determined fixed weights $w_i = 1/m$, see Eq.(4.2).
3. "Robust" optimization using a second-order second-moment approximation around the mean value $M = 0.75$, see Eq.(5.4).
4. "Robust" optimization using stochastic integration. To allow for a direct comparison with the multipoint results, $f_M(M)$ in Eq.(5.1) is a uniform distribution. Other distributions are considered as well, which demonstrates the versatility of the expected value optimization method.

It is important to note that formulation 2 and 4 require a comparable computational effort.

6.2. Single-Point Optimization Results. The single point case has 21 design variables: the angle of attack α and the vertical positions of the 10 spline control nodes at both the top and bottom surface of the airfoil. Figure 4.1a indicates a dramatic reduction of the drag C_d is obtained at $M = 0.76$ (also see the first entry in Table 6.1), but also reveals that this gain is rapidly lost when the free flow Mach number is away from this design value.

TABLE 6.1

Comparison of the drag reductions with respect to the original NACA-0012 at the design point and over the entire Mach range for single point optimization results.

Optimization model	Grid	Target lift C_l^*	Design Mach number M	ΔC_d at the design point	Actual total reduction ΔC_d
CONMIN	Grid 2	0.175	0.76	44%	12%
PORT	Grid 1	0.175	0.75	24%	11%
SLP/ADS	Grid 2	0.2	0.75	49%	21%
SLP/ADS	Grid 2	0.2	0.76	60%	18%
SLP/ADS	Grid 2	0.4	0.75	84%	52%
SLP/ADS	Grid 2	0.6	0.72	85%	30%
SLP/ADS	Grid 2	0.6	0.75	87%	53%
SLP/ADS	Grid 2	0.6	0.78	91%	78%
SLP/ADS	Grid 2	0.6	0.80	75%	57%

The geometry plot in Figure 4.1b illustrates what happens. During the optimization a distinct "bump" is formed on the airfoil surface. The optimizer takes advantage of all degrees of freedom to achieve the lowest possible drag at the design Mach number $M = 0.76$, irrespective of what happens to the drag at other Mach numbers. Obviously, there is a penalty to be paid for this: even though the drag reduction at the design Mach number is 44%, the total average reduction over the entire Mach range is only 12% (results obtained with Grid 2 and $C_l^* = 0.175$ using the CONMIN optimizer implemented in the iSIGHT package

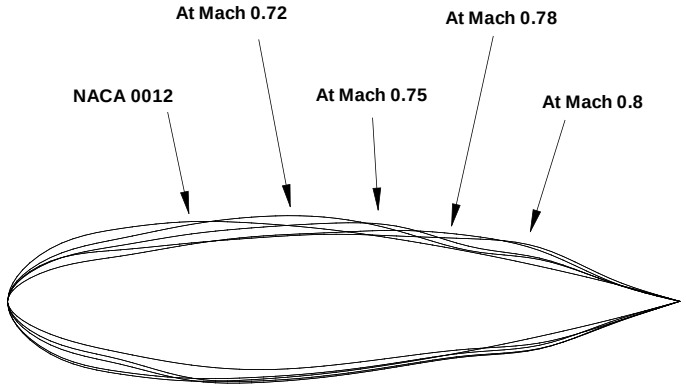

FIG. 6.1. *Bump locations for different design Mach numbers for single point optimization (results obtained using Grid 2, $C_l^* = 0.6$, and SLP/ADS [22] optimizer)*

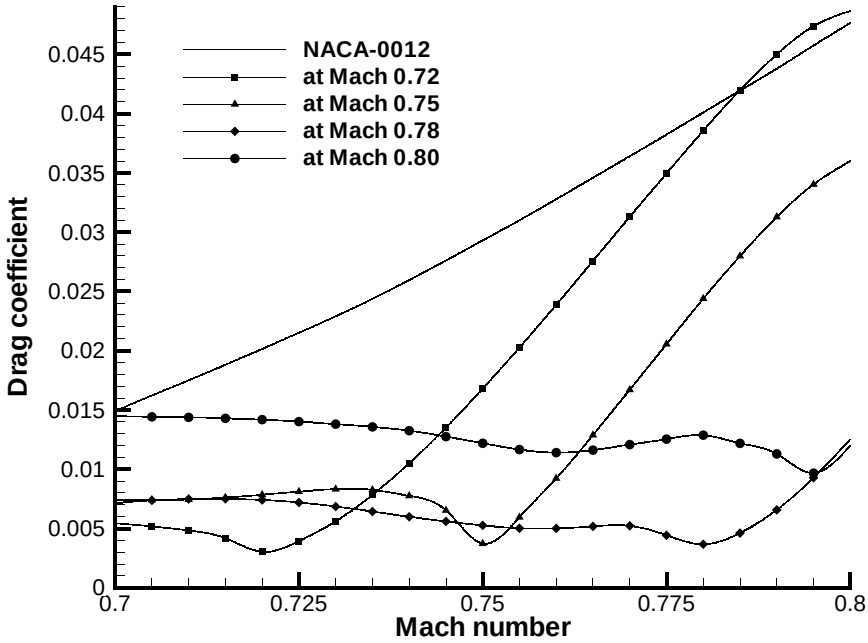

FIG. 6.2. *Single point optimization results for various design Mach numbers (results obtained using Grid 2, $C_l^* = 0.6$, and SLP/ADS [22] optimizer)*

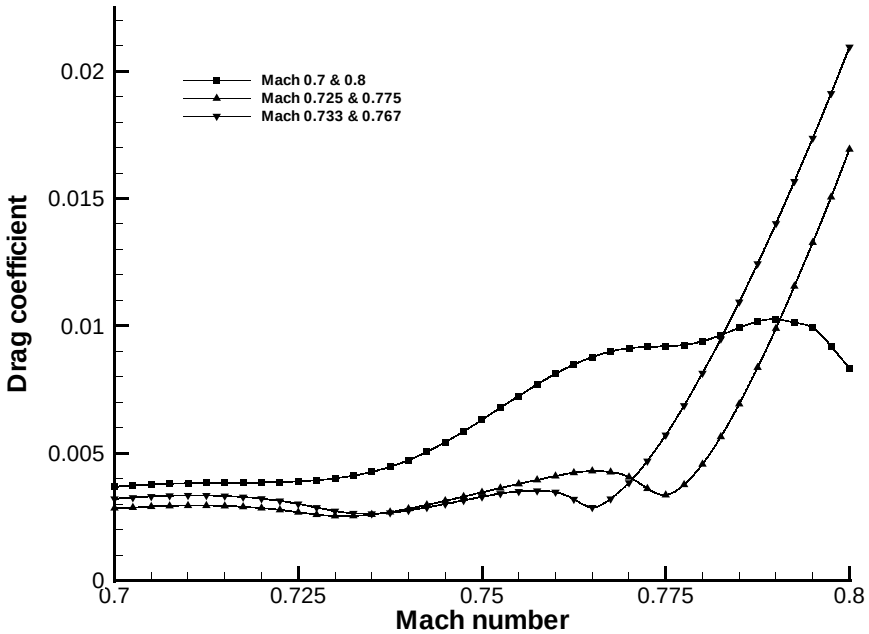

FIG. 6.3. *Optimal drag profiles obtained using different 2-point optimization schemes (results obtained using Grid 2, $w_1 = w_2 = 0.5, C_l^* = 0.6$ and SLP/ADS optimizer)*

[11]). The use of a single-point optimization would lead to the false conclusion that a 44% improvement has been achieved; the actual realized gain is only 12%.

When unconstrained optimization using PORT [14] after elimination of the lift constraint is used (results for Grid 1 and $C_l^* = 0.175$), the drag reduction at the design Mach number $M = 0.75$ is 24% and the actual reduction over the entire Mach range is found to be 11%. It can be concluded that both methods to handle the constraints lead to the same qualitative result. The numerical difference between the two results can be attributed to the overestimation of the drag of the baseline NACA-0012 in Grid 1, which results in a larger reduction in the optimized profile.

Qualitatively similar results are obtained for other lift values and design Mach numbers and are summarized in Table 6.1. The localized optimization, illustrated in Figure 4.1, was previously documented by Drela [9]. Figure 6.1 shows that the bump on the airfoil moves aft when the Mach number increases. This pushes the shock towards the trailing edge and postpones the drag rise. Figure 6.2 indicates that the choice of the design Mach number considered in the optimization has an enormous impact on the final drag profile and airfoil geometry. The figure shows that simply selecting the average Mach number (so called Mean-Value Optimization at $M = 0.75$) or the Mach number with highest drag ($M = 0.80$) does not guarantee good overall performance over the entire Mach range.

6.3. Multi-Point Optimizations. The constrained multi-point optimization has $20 + m$ design variables: the same 20 y-coordinates which describe the geometry and m angles of attack. The minimum angle of attack for which the lift constraint is satisfied, decreases with increasing free flow Mach number due to compressibility effects [21]. Consequently, each design condition adds one additional angle-of-attack design

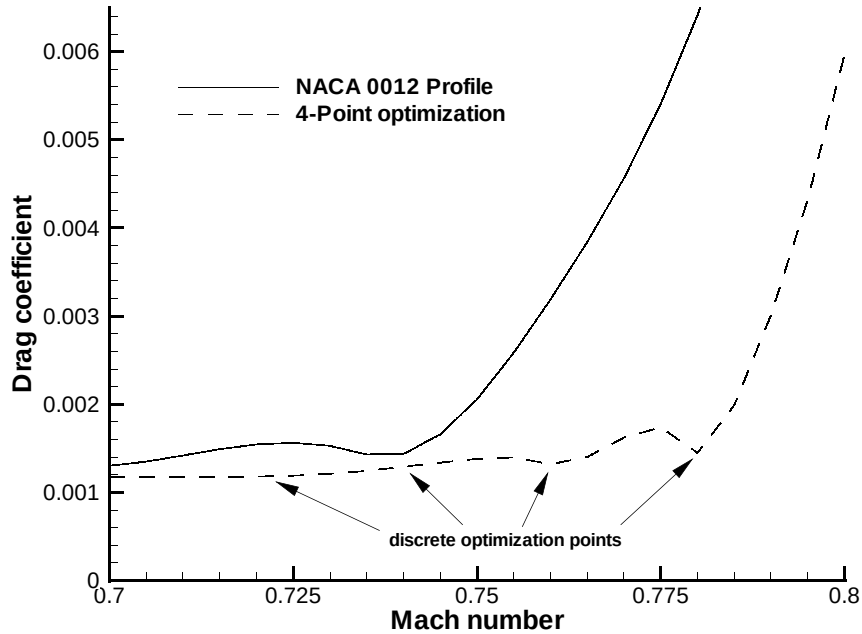

FIG. 6.4. *Drag profile obtained using 4-point optimization strategy (results obtained using Grid 2,* $M_i = 0.72, 0.74, 0.76$ *and* $0.78, w_i = 0.25, C_l^* = 0.175$*, and CONMIN optimizer)*

variable.

The two-point optimization results shown in Figure 6.3 illustrate the shortcomings reported by Drela [9]. Optimization at selected Mach numbers results in clearly distinguishable drag troughs at each of the design Mach numbers (see also Figures 6.4, 4.2 and 4.3). Drela leaves it up to the designer to determine which Mach numbers to include in the objective in Eq. (4.2) and what weights to choose. Three "reasonable" selections are compared with each other in Figure 6.3 and it is clear that, at least in this case, the selection of the design conditions has an important effect on the final results. In particular the selection of the endpoints of the Mach range can lead to troubling results. We observed this in both 2-point (Figure 6.3) and 4-point (Figure 6.4) optimization.

Since the drag is higher in the upper part of the Mach range, one may want to include more design Mach numbers from the upper part than from the lower part in the multi-point objective Eq.(4.2). This procedure does not require any additional function calls and consequently keeps the computational cost under control and should result in lower drag at the upper end of the Mach range. Figure 6.5 shows the result of such a multi-point optimization. The selected Mach numbers are indicated on the chart and the weights w_i are obtained from the numerical integration using 4 fixed integration points. It can be concluded that the maximum drag is indeed reduced, but a substantial penalty is to be paid near the lower end of the Mach range. As a matter of fact the expected value of the drag has actually increased from 0.0044 to 0.0055 (assuming a uniform distribution for the Mach numbers between 0.7 and 0.8) compared with the result for evenly spaced Mach numbers. Also, the distinct multiple drag troughs at each of the sample Mach numbers persist, which indicates "localized optimization" as explained earlier.

All these results indicate that a multi-point optimization does indeed achieve a better overall drag

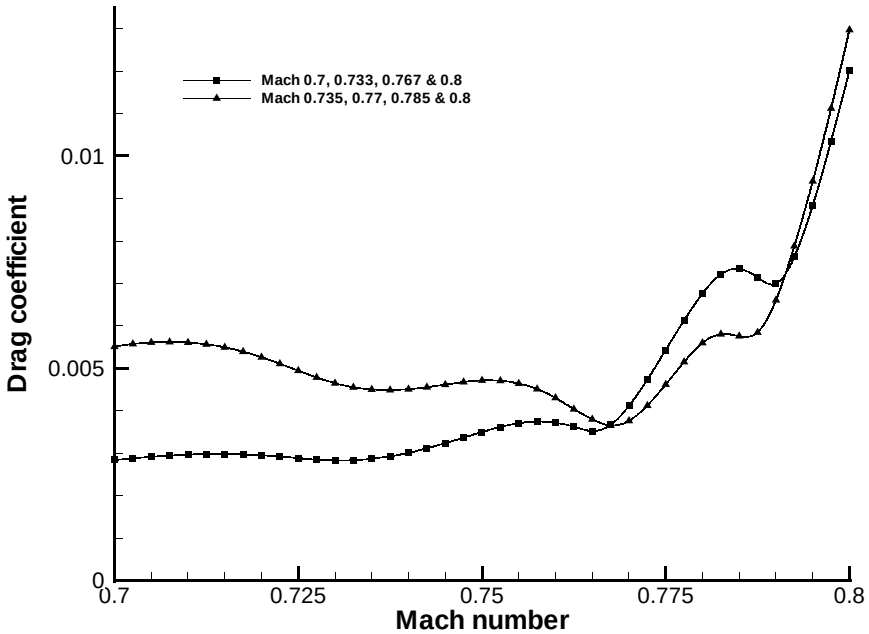

FIG. 6.5. *Drag profile obtained using different 4-point optimization strategies (results obtained using Grid 2, $C_l^* = 0.6$, and SLP/ADS optimizer)*

reduction for both methods. This is in line with the findings of other researchers [9]. However, a drag-trough is formed at or near each of the discrete design points. The drag increases rapidly away from the design points. This is very clear near the high end of the Mach range.

6.4. Expected Value Optimization. Figure 6.6 shows that the expected value optimization strategy results in a much smoother drag profile over the entire Mach range. The integration of the drag over the Mach range is performed using spline-based inter/extrapolation. The resulting airfoil geometry is a lot smoother as well. It can be concluded that this scheme results in a superior design for an identical computational effort.

For the expected value scheme the integration points in Eq.(5.1) are altered slightly for each optimization iteration. Consequently, we can say that the 4-point optimization minimizes a weighted sum of 4 fixed design conditions, whereas the robust scheme minimizes the weighted sum of *any* 4 design conditions. This avoids "localized optimization". In this study a random perturbation scheme is used to change the integration points, but other, more adaptive strategies are currently being researched. The number of integration points must be sufficiently high so that the integration error caused by the change of integration points between optimization steps is smaller than the decrease of drag in that particular optimization step (cfr. supra).

In his study, Drela [9] applies larger weights to the upper part of the Mach range to ensure "that the upper part is not compromised excessively by the less important lower part". Our statistical decision approach suggests that this can only be justified when the higher Mach numbers are more likely to occur, i.e. when the PDF $f_M(M)$ is concentrated in the upper Mach range. The weights follow automatically from the integration procedure and are as such not directly linked to the actual values of the drag $C_d(M)$.

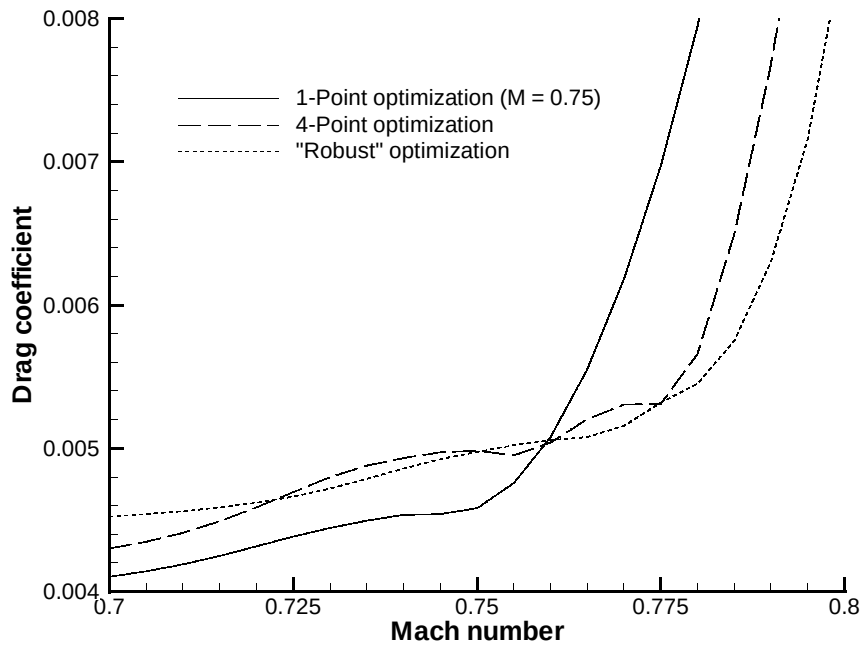

FIG. 6.6. *Drag profile obtained using different optimization strategies (results obtained using Grid 1,* $C_l^* = 0.175$ *and PORT optimizer)*

6.5. Impact of PDF. In most practical cases the Mach number will not be uniformly distributed over a given range. A key advantage of the explicitly statistical approach is that the relative importance of each operating condition is automatically accounted for through the PDF.

Quite often a cruise Mach number is set and the assumption of a (truncated) "normal" or Gaussian distribution around this mean value seems appropriate. The truncated normal PDF is very well approximated by a Beta distribution. The Beta distribution is always bounded within an interval $[a, b]$ and has shape parameters α_1 and α_2, both greater than zero:

$$Beta(x, a, b, \alpha_1, \alpha_2) = \frac{\left(\frac{x-a}{b-a}\right)^{(\alpha_1-1)} \left(\frac{b-x}{b-a}\right)^{(\alpha_2-1)}}{(b-a) \times B(\alpha_1, \alpha_2)} \tag{6.1}$$

where $B(\alpha_1, \alpha_2) = \Gamma(\alpha_1)\Gamma(\alpha_2)/\Gamma(\alpha_1 + \alpha_2)$ is the Beta-function.

Depending on the value of α_1 and α_2, the Beta PDF can assume a variety of shapes (see Figure 6.8). When $\alpha_1 = \alpha_2$ the distribution is symmetric and can be used as an approximation for the truncated normal, especially for $\alpha_i \geq 5$. When $\alpha_1 = \alpha_2 = 1$, the distribution becomes uniform. For $\alpha_1 \neq \alpha_2$ the distribution is skewed towards either left or right. Bath-tub distributions are obtained when both parameters in the PDF are less than 1 (but greater than 0).

Figure 6.9 compares the optimal drag-profile obtained using three different Beta-distributions bounded within $[0.7, 0.8]$. When a PDF $Beta(3, 1)$ is assumed for the Mach number, the higher Mach numbers are more likely to occur. Their impact is easily discerned from Figure 6.9. The greater weight of the higher Mach numbers translates into a lower drag in the high Mach range. The trade-off is a higher drag at the

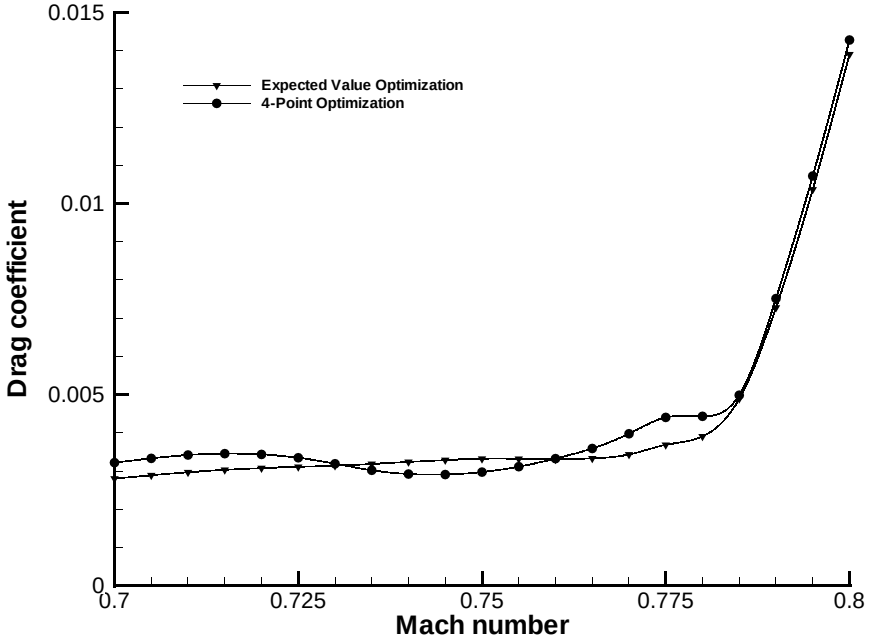

FIG. 6.7. *Drag profile obtained using different optimization strategies (results obtained using Grid 2, $C_l^* = 0.6$ and SLP/ADS optimizer)*

lower end of the Mach range. For a $Beta(1,3)$-distribution, a lower drag is obtained in the lower part of the Mach range at the expense of much faster drag increase for higher Mach numbers. When a $Beta(5,5)$ PDF is used, the higher likelihood of Mach numbers near the mean value $M = 0.75$ results in the lowest drag of all three curves near the middle of the Mach range. The corresponding airfoil geometries are shown in Figure 6.10.

This illustrative comparison reveals the importance of an accurate quantification of the PDF of the Mach range. In general, careful data analysis is required when the PDF is selected for each of the uncertain variables. Practical experience has revealed that especially the tails of the distributions need to be modeled very carefully because they tend to have a large impact [17]. Cut-off values should most definitely not be chosen arbitrarily!

6.6. Approximate Second-Order Second-Moment Method (SOSM). In this section we present results using the deterministically equivalent problem formulation Eq.(5.4), which is based on a second-order analytic approximation of Eq.(5.1).

Eq.(5.4) indicates that first-order sensitivities of the drag C_d with respect to the uncertain variable M do not affect the expected value of the design. The second-order information represents the curvature of the $C_d(M)$ Mach sweep, which is indicative of "localized optimization". In the SOSM formulation, the weighting between the drag and the curvature is determined by physics: it is given by the variance of the Mach number. Figure 6.11 shows a considerable improvement in the robustness of the design.

The drag reduction is not quite as good as obtained using explicit numerical integration (Figure 6.7), but the computational effort is a lot smaller. The method is particularly useful if higher order derivatives

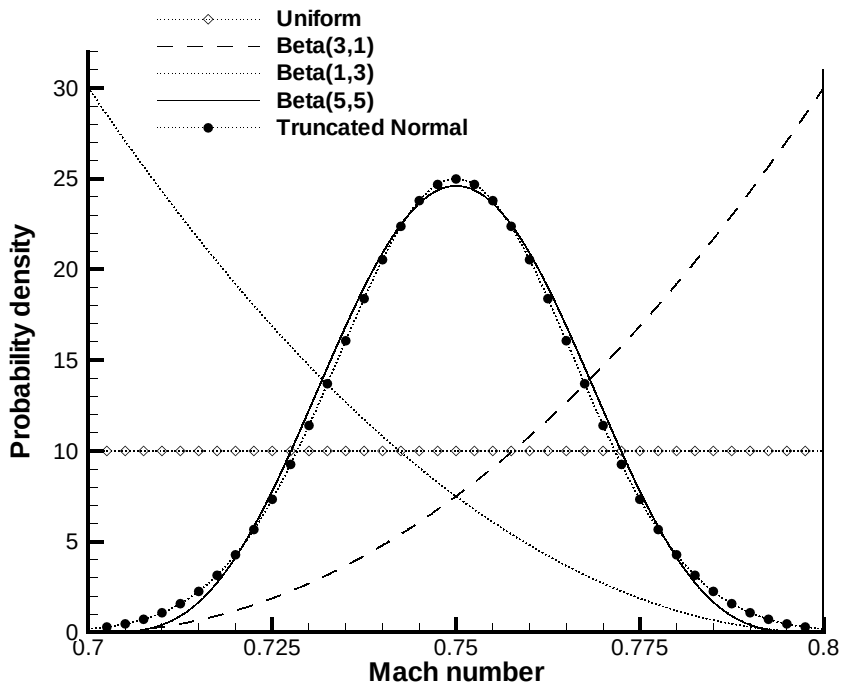

FIG. 6.8. *Sample Beta distributions, and comparison with truncated Normal*

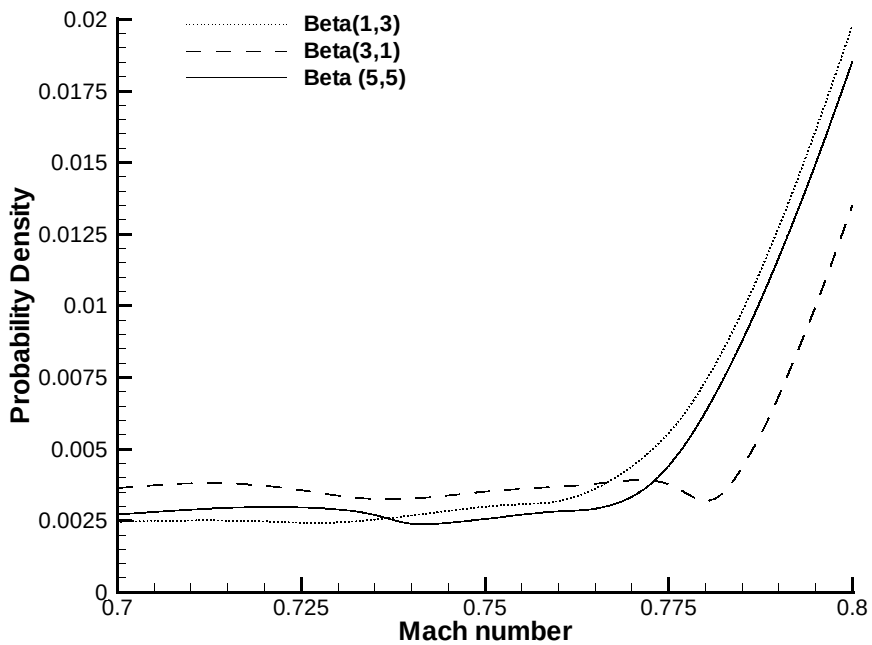

FIG. 6.9. *Impact of assumed PDF for M on optimal drag profile (grid 2, $C_l^* = 0.6$ SLP/ADS optimizer)*

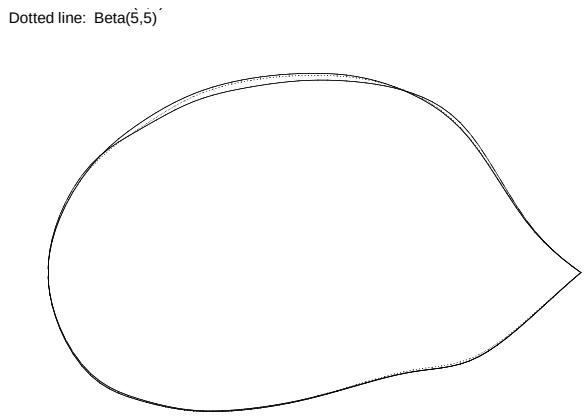

FIG. 6.10. *Airfoil geometries for three Mach distributions (grid 2, $C_l^* = 0.6$ SLP/ADS optimizer)*

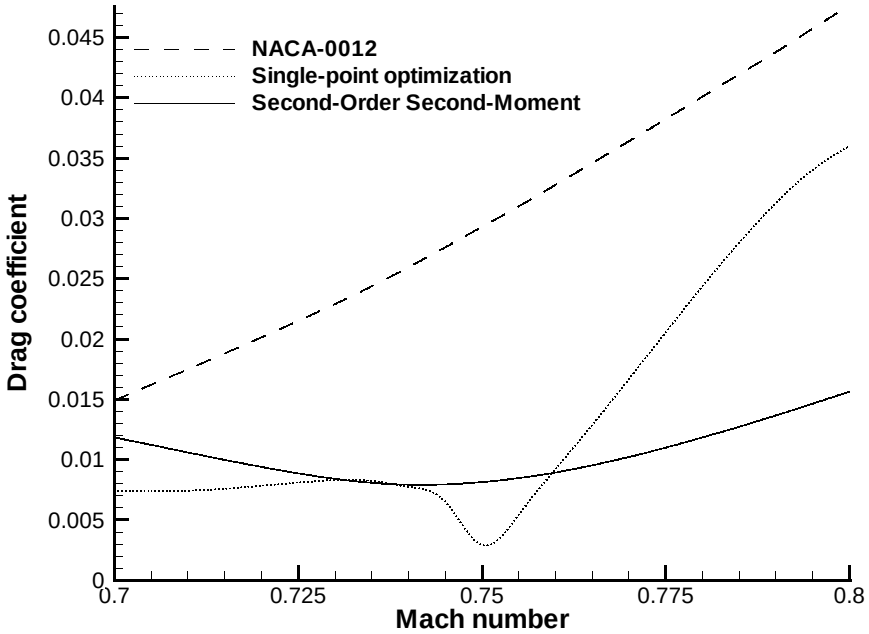

FIG. 6.11. *Comparison of SOSM result with single-point optimization (grid 2, $C_l^* = 0.6$ SLP/ADS optimizer)*

are available (and numerically reliable) and several uncertain variables are present in the problem. Table 6.6 compares the relative computational cost. SOSM scales linearly with the number of random variables, whereas full numerical integration may rapidly become prohibitively expensive. Because the method is based

TABLE 6.2

Number of function/derivative evaluations required per optimization step (Note: SOSM requires less if analytic derivatives are available)

Optimization Method	1 Random Variable	3 Random Variables
Single Point	1	1
SOSM	3	7
Expected Value (using 4-point integration)	4	64

on a second-order approximation of the objective function, SOSM will give the best results if the variance of the random variables is relatively small.

7. Summary and Conclusions. The robustness of an optimal solution can be achieved by incorporating the variability of the operating conditions directly into the optimization problem formulation. The practical application shows that a statistical approach leads to smooth airfoil geometries and drag profiles.

The suggested expected value optimization method is computationally similar to existing multi-point optimization, which is widely accepted in industry. This increases the likelihood of acceptance by both designers and theorists alike. The new formulation avoids the arbitrary selection of design conditions and weighting factors; they automatically follow from the procedure.

A second-order second-moment approximate integration provides additional insight into the problem. SOSM scales linearly with the number of design variables and may be the only feasible alternative when a lot of uncertainties are considered. This will be the focus of future research.

The relative likelihood of each operating condition is directly taken into account. The importance of a careful selection of the PDF is illustrated by means of an example. A randomized integration scheme ensures that the optimizer cannot exploit approximation errors due to discretization. Further research into different sampling schemes is required.

It can be concluded that airfoil shape optimization on the basis of the Euler equations leads to some interesting candidate designs. However, viscous effects need to be included to achieve more realistic pressure distributions.

Acknowledgements. The author is indebted to Sharon L. Padula of the NASA Langley Research Center's Multidisciplinary Optimization Branch, William A. Crossley of the Purdue University School of Aeronautics and Astronautics and Wu Li of Old Dominion University for their insightful comments and suggestions and to Eric J. Nielsen of the NASA Langley Research Center's Computational Modeling and Simulations Branch for his help with both the FUN2D code and the various grid generators. The author also wishes to acknowledge the contribution of R. Michael Lewis of the College of William and Mary, who first suggested this optimization problem.

REFERENCES

[1] G.H. ABUMERI, L.H. KUGUOGLU AND C.C. CHAMIS, *Non-deterministic optimization - Composite laminates, beams and blades*, 41st AIAA/ASME/ASCE/AHS/ASC Structures, Structural Dynamics, and Materials Conference and Exhibit, Atlanta, GA, 2000.

[2] N.M. Alexandrov, R.M. Lewis, C.R. Gumbert, L.L. Green, and P.A. Newman, *Optimization with Variable-Fidelity Models Applied to Wing Design*, AIAA-2000-0841, accepted for publication in AIAA Journal of Aircraft. Also available as ICASE technical report 99-49, 2000.

[3] W.K. Anderson and D.L. Bonhaus, *Airfoil Design on Unstructured Grids for Turbulent Flows*, AIAA Journal, 37(2) (1999), pp. 185-191.

[4] W.K. Anderson and D.L. Bonhaus, *An Implicit Upwind Algorithm for Computing Turbulent Flows on Unstructured Grids*, Computers and Fluids, 23(1) (1994), pp. 1-21.

[5] S.M. Batill, J.E. Renaud and X. Gu, *Modeling and Simulation Uncertainty in Multidisciplinary Design Optimization* AIAA-2000-4803, 2000.

[6] R.L. Campbell, *Efficient Viscous Design of Realistic Aircraft Configurations*, AIAA-98-2539, 1998.

[7] M.C. Chiao and C.C. Chamis., *Optimization of Adaptive Intraply Hybrid Fiber Composites with Reliability Considerations*, NASA TM-106632, NASA Glenn Research Center, Cleveland, OH, 1994.

[8] M. Drela, *Low Reynolds number airfoil design for the MIT Daedalus prototype: A case study*, Journal of Aircraft, 25(8) (1988), pp. 724-732.

[9] M. Drela, *Pros & Cons of Airfoil Optimization*, Frontiers of Computational Fluid Dynamics, 1998.

[10] J. Elliott and J. Peraire, *Constrained, Multipoint Shape Optimization for Complex 3D Configurations*, Aeronautical Journal, 102(1017) (1998), pp. 365-376.

[11] Engineous Software, *iSIGHT: Designer's Guide*, Version 5.5, 2000.

[12] W.Y. Fowlkes and C.M. Creveling, *Engineering Methods for Robust Product Design Using Taguchi Methods in Technology and Product Development*, Addison-Wesley, Reading, MA, 1995.

[13] X. Gu, J.E. Renaud, S.M. Batill, R.M. Brach and A.S. Budhiraja, *Worst case propagated uncertainty of multidisciplinary systems in robust design optimization.* Structural and Multidisciplinary Optimization, 20(3) (2000), pp. 190-213.

[14] L. Kaufman and D. Gay, *PORT Library: Optimization and Mathematical Programming*, Bell Laboratories, 1997.

[15] J. Loncaric, *http://www.icase.edu/CoralProject.html*, ICASE, NASA Langley Research Center, 2001.

[16] H.O. Madsen, S. Krenk and N.C. Lind, *Methods of Structural Safety*, Prentice-Hall, Englewood Cliffs, NJ, 1986.

[17] M.A. Maes and L. Huyse, *Tail Effects of Modeling Uncertainty in Risk and Reliability Analysis*, Third International Symposium on Uncertainty Modeling and Analysis, College Park, MD, 1995, pp. 133-138.

[18] D.L. Marcum, *Generation of Unstructured Grids for Viscous Flow Applications*, AIAA 95-0212, 1995.

[19] E.J. Nielsen and W.K. Anderson, *Recent Improvements in Aerodynamic Design Optimization On Unstructured Meshes*, AIAA-2001-0596, 2001.

[20] J.W. Pratt, H. Raiffa, and R. Schlaifer, *Introduction to Statistical Decision Theory*, MIT Press, Cambridge, MA, 1996.

[21] R.S. Shevell, *Fundamentals of Flight*, Prentice-Hall, Englewood Cliffs, NJ, 1989.

[22] G.N. Vanderplaats, *ADS - A FORTRAN Program for Automated Design Synthesis*, Engineering Decision Optimization, Santa Barbara, CA, 1987.

[23] W.L. Winston, *Operations Research - Algorithms and Applications*, Third Edition, Duxbury Press, Belmont, CA, 1994.